ARTICLE

Enhanced Surface Plasmon Resonance on a Smooth Silver Film with a Seed Growth Layer

Hong Liu,[†] Bing Wang,[†] Eunice S. P. Leong,[†] Ping Yang,[‡] Yun Zong,[†] Guangyuan Si,[§] Jinghua Teng,[†,]* and Stefan A. Maier[⊥,]*

[†]Institute of Materials Research and Engineering, Agency for Science, Technology and Research (A*STAR), 3 Research Link, Singapore 117602, [‡]Singapore Synchrotron Light Source (SSLS), National University of Singapore, 5 Research Link, Singapore 117603, [§]Department of Electrical and Computer Engineering, National University of Singapore, 4 Engineering Drive 3, Singapore 117576, and [⊥]Department of Physics, Imperial College London, London SW7 2AZ, U.K.

ABSTRACT This paper reports an effective method to enhance the surface plasmon resonance (SPR) on Ag films by using a thin Ni seed layer assisted deposition. Ag films with a thickness of about 50 nm were deposited by electron beam evaporation above an ultrathin Ni seed layer of ~2 nm on both silicon and quartz substrates. The root-mean-square (rms) surface roughness and the correlation length have been reduced from >4 nm and 28 nm for a pure Ag film to ~1.3 and 19 nm for Ag/Ni films, respectively. Both experimental and simulation results show that the Ag/Ni films exhibit an enhanced SPR over the pure Ag film with a narrower full width at half-maximum. Ag films with a Ge seed layer have also been prepared under the same conditions. The surface roughness can be reduced to less than 0.7 nm, but narrowing of the SPR curve is not observed due to increased absorptive damping in the Ge seed layer. Our results show that Ni acts as a roughness-diminishing growth layer for the Ag film while at the same time maintaining and enhancing the plasmonic properties of the combined structures. This points toward its use for low-loss plasmonic devices and optical metamaterials applications.

KEYWORDS: surface plasmon resonance · metamaterials · silver · nickel · germanium · surface roughness

In recent years, new efforts to create ultrasmooth silver thin films have been driven by the increasing demands imposed by the development of plasmonic nanodevices and metamaterials.[1−3] Silver has been the most frequently employed metal for plasmonic devices,[4] cavities,[5] and metamaterials,[6,7] benefiting from its competitive intrinsic properties compared to all other practical metals, such as its low contact resistance and low refractive index (~0.1),[8] the low damping and hence low loss,[9] and high reflectivity[10] in the visible wavelength region. Nevertheless, silver films deposited by conventional methods exhibit a rather rough surface resulting in a significant surface plasmon polariton scattering loss, which exposes a major impediment to achieving higher optical quality and lower-loss plasmonic devices and metamaterials.[11] The inhomogeneity of the surface morphology sensitively influences the surface plasmon resonance at the metal−dielectric interface, giving rise to performance degradation.

Ag films deposited by conventional techniques, including electron beam evaporation,[11] chemical vapor deposition,[12] electroless plating,[13] and sputtering,[14,15] are usually polycrystalline as they tend to grow in Volmer−Weber mode,[16] which leads to a surface roughness at 2 nm and above in terms of root-mean-square (rms). In recent years, several new fabrication techniques have been exploited aiming to obtain Ag films with subnanometer scale roughness. A mechanical imprinting technique has been developed by applying a pressure of ~600 MPa on a 100-nm thick Ag film deposited on a silicon substrate by electron beam evaporation. A remarkable ultrasmooth plane of less than 0.1 nm rms roughness has been demonstrated in a 100 μm by 100 μm imprinted pattern.[17] However, both the stability and reproducibility of this technique still need further investigation, and it may be difficult to apply for large-area fabrication. Using a combination of template stripping and patterning on silicon substrates, a 0.34-nm roughness (rms) for a 30-nm thick and thermally evaporated silver film has also been reported.[18] A simpler method to make ultrasmooth Ag films has been reported by employing a thin Ge seed layer with a thickness of 0.5−15 nm, deposited *via* e-beam evaporation on Si(100) substrates.[19] A dramatic improvement of surface roughness down to about 0.6 nm (rms) has been achieved.

Our study has been motivated to find a seed layer material which is able to not only create an ultrasmooth Ag film, but also to improve its surface plasmon resonance (SPR) for plasmonic and metamaterials

*Address correspondence to jh-teng@imre.a-star.edu.sg, s.maier@imperial.ac.uk.

Received for review March 8, 2010 and accepted May 20, 2010.

Published online June 1, 2010.
10.1021/nn100466p

© 2010 American Chemical Society

TABLE 1. Thickness of Each Layer for All Samples Measured by Ellipsometry

	Sample 1—Ag/Ni	Sample 2—Ag/Ge	Sample 3—Ag
thickness (nm)	Ag: 56.84	Ag: 52.72	Ag: 54.56
	Ni: 2.7	Ge: 1.4	
mean square error (MSE)	1.806	1.691	1.13

applications. At the same time, this proposed material should be capable of promoting the adhesion of silver to substrates for practical applications, since it is known that silver exhibits poor adhesion to semiconductors. Ni is one of the commonly used adhesion layers and its metallic properties would be able to enhance the SPR of Ag/Ni films. On the other hand, Ge as a seed layer has been reported to be able to significantly reduce the roughness of silver, but without any report on its optical and plasmonic properties. In this paper, both Ag/Ni and Ag/Ge films are investigated in terms of surface plasmon resonance through experimental and theoretical means, as well as compared with a pure Ag film.

We deposited Ag films of about 50-nm thickness over a thin 2 nm seed layer of Ni and Ge, respectively, on both Si(100) and quartz substrates by electron beam evaporation. The surface morphology and rms surface roughness were characterized by atomic force microscopy (AFM). Variable angle spectroscopic ellipsometry was used to characterize film thickness, in addition to high resolution X-ray reflectometry (HR-XRR). The purpose of using both ellipsometry and HR-XRR was to cross-examine the film thickness, which is one of the critical parameters in this study. Measurement and modeling of surface plasmon resonance (SPR) spectroscopy have been carried out using a prism coupling method. The deposited Ag films over Ni and Ge seed layers are denoted as Sample 1 and Sample 2, respectively, while the Ag film without any seed layer is denoted as Sample 3.

RESULTS AND DISCUSSION

Table 1 lists the thickness of each layer and its corresponding mean square error (MSE) measured by ellipsometry for Samples 1−3. The results of thickness measurement for all samples characterized by ellipsometry and HR-XRR are identical with negligible discrepancy. It shows that Ni, Ge, and Ag films have been deposited with the desired thicknesses, which have been measured with satisfactory MSEs of less than 2. Figure 1 shows the surface morphologies of Samples 1−3 characterized by AFM on silicon substrates a, c, and e, and on quartz substrates b, d, and f, respectively. Table 2 lists the rms surface roughness, grain sizes and peak-to-peak values of all samples from AFM characterization. As shown in Figure 1 panels a and b, Sample 1 of the Ag/Ni films presents an improved rms surface roughness varying from 1.3 to 1.7 nm in a 1 μm^2 area on both silicon and quartz. Figure 1 panels c and d plot ultrasmooth surfaces of Ag/Ge films with an rms roughness of about 0.7 nm, which are in agreement with the results reported recently.[19] Sample 3, as shown in Figure 1 panels e and f, exhibits comparatively rough surfaces of rms roughness above 4 nm as expected. Additionally, Sample 1 exhibits grain sizes of about 15/12 nm and peak-to-peak heights of about 0.2/0.1 nm on both substrates, which are correspondingly about 6/4 nm and 0.04/0.03 nm for Sample 2. In contrast to Samples 1 and 2, Sample 3 has relatively larger grain sizes of ~17/15 nm and a

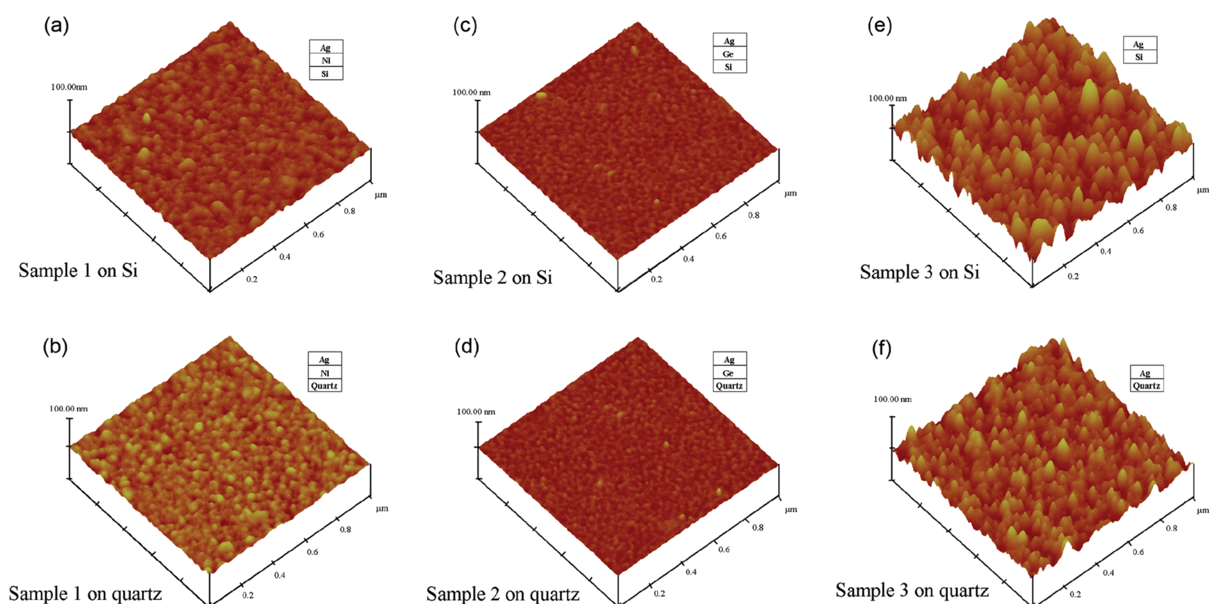

Figure 1. AFM images of Samples 1−3. The rms surface roughness measured for Sample 1 is (a) 1.752 nm on silicon and (b) 1.323 nm on quartz; for Sample 2 (c) 0.705 nm on silicon and (d) 0.694 nm on quartz; for Sample 3 (e) 8.094 nm on silicon and (f) 4.548 nm on quartz, respectively. (Insets schematically show the layer structures of Samples 1−3.)

TABLE 2. Surface Roughness (rms) of Samples 1, 2, and 3 Characterized by AFM on Silicon and Quartz Substrates

	AFM measurement results						calculation results	
	surface roughness (nm)		grain size (nm)		peak-to-peak height (nm)		correlation length σ (nm)	surface roughness δ (nm)
	on silicon	on quartz	on silicon	on quartz	on silicon	on quartz	on quartz	on quartz
Sample 1, Ag/Ni	1.752	1.323	15.354	11.890	0.198	0.101	19.0	1.3
Sample 2, Ag/Ge	0.705	0.694	5.840	4.219	0.041	0.028	11.2	0.7
Sample 3, Ag	8.094	4.548	16.564	14.548	0.678	0.460	28.2	4.5

peak-to-peak height of ~0.45/0.65 nm on silicon and quartz substrates, respectively. The AFM results hence show that a thin layer of Ni on quartz has remarkably improved the smoothness of the film by up to 3-fold, while the improvement is more than 6-fold for a thin layer of Ge in comparison with the pure Ag film.

To characterize the surface roughness, the rms height δ and correlation length σ are two important quantities. They can be derived from the correlation function

$$G(r) = 1/S \int_s \varsigma(r')\,\varsigma(r' + r)\,dr' \qquad (1)$$

where $\varsigma(r)$ denotes the height distribution of roughness, $r = (x,y)$ represents the coordinate, and S is the area of the surface with roughness. In a computational implementation, $G(r)$ can be numerically calculated by

$$G(r) = F^{1}\{F^{1}\{\varsigma(r)\}F\{\varsigma(r)\}\} \qquad (2)$$

where F and F^{-1} represent the discrete Fourier transform and inverse discrete Fourier transform, respectively. Statistically assumed to follow a Gaussian distribution, the correlation function can be written as

$$G(r) = \delta^2 \exp(-r^2/\sigma^2) \qquad (3)$$

By fitting the numerical data with the Gaussian function, the surface roughness δ and correlation length σ can be extracted. We note that the roughness values of Samples 1−3 obtained by the analytical method are equal to the AFM measurement results.

Figure 2 plots the correlation functions of surface roughness and the corresponding Gaussian fittings to obtain the correlation length δ and surface roughness σ for Samples 1−3, respectively. The sizes of bright spots of the correlation function as shown in Figure 2 panels a, c, and e are proportional to the respective roughness magnitudes. Sample 1 exhibits the medium correlation length, Sample 2 exhibits the smallest, while Sample 3 exhibits the largest one, which is matching to the order of their roughness magnitudes. As shown in Figure 2b, d, f, the magnitude of the Gaussian fitting at the origin represents δ^2, while the full width at half-maximum (FWHM) of the fitted curve represents the

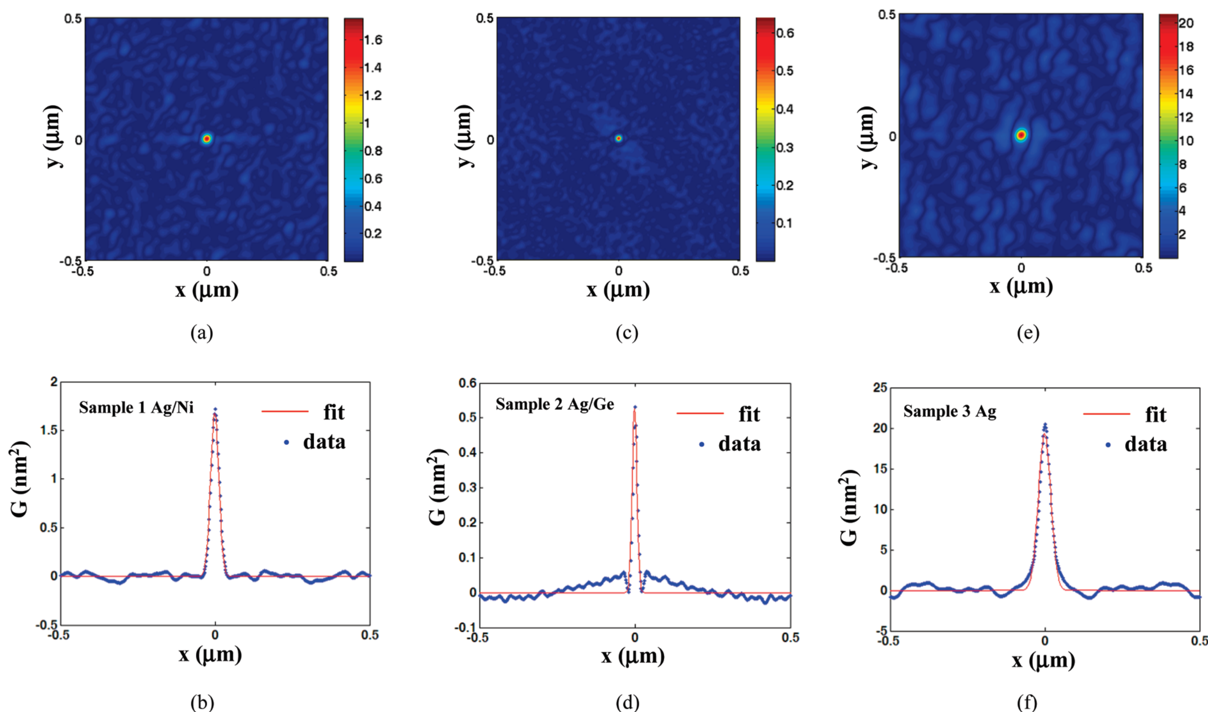

Figure 2. The correlation functions of the surface roughness for (a) Sample 1, (c) Sample 2, and (e) Sample 3, and the corresponding Gaussian function fittings to extract the correlation length δ and surface roughness σ for (b) Sample 1, (d) Sample 2, and (f) Sample 3.

correlation length σ for each sample. The correlation length σ is theoretically comparable with the typical lateral magnitude of roughness. Sample 2 shown in Figure 2d exhibits the smallest lateral size, while Sample 3 exhibits the largest. All these results corroborate a decrease in roughness going from no seed layer to Ni and Ge, respectively.

Surface plasmon resonance (SPR) spectroscopy measurements and theoretical calculations have been performed to evaluate the effects of the Ni and Ge seed layers on the SPR of the Ag films. The data for theoretical calculations, such as thickness and rms roughness of each sample were taken from measurement results listed in Tables 1 and 2, while the corresponding dielectric constants were taken from the literature.[20] To differentiate the surface roughness effect, ideal surfaces without taking surface roughness into account have also been employed in theoretical calculations for all samples. To analyze their effects quantitatively and compare their overall performance qualitatively, key features of the SPR reflectivity curves including resonance angle, angular FWHM, and figure of merit (FOM) are studied. For extinction-based SPR, smaller FWHM and larger peak amplitude are desirable because a deeper and narrower resonance spectrum offers a higher efficiency and sensitivity. The FOM, which is proportional to the sensitivity to SPR, is defined here as

$$\mathrm{FOM} = \frac{\Delta R}{R_c}\frac{1}{\mathrm{FWHM}} \qquad (4)$$

where ΔR is the difference of reflectivity between the critical angle and resonance angle, while R_c is the reflectivity at the critical angle.

The theoretical calculation of reflection spectrum of SPR can be achieved from Fresnel's equations

$$R = \left|\frac{Z_{\mathrm{in},1} - Z_0}{Z_{\mathrm{in},1} + Z_0}\right|^2 \qquad (5)$$

where R is the reflectivity. The input impedance at intermediate layer n is given by $Z_{\mathrm{in},n} = Z_n[Z_{\mathrm{in},n+1} - \mathrm{i}Z_n \tan(k_n d_n)][Z_n - \mathrm{i}Z_{\mathrm{in},n+1} \tan(k_n d_n)]^{-1}$, with $Z_n = k_n/\varepsilon_n k_0$, $Z_{\mathrm{in,M}-1} = Z_{\mathrm{M}-1}$, $k_n = (\varepsilon_n k_0^2 - k_x^2)^{1/2}$, $k_x = k_0 n_p \sin(\theta)$, $k_0 = 2\pi/\lambda$. The variable n denotes the index of the metal or dielectric layer, $n_p = \varepsilon_0^{1/2}$ is the refractive index of the prism, M is the total number of layers, λ is the wavelength, d_n is the thickness of the nth layer with ε_n as its dielectric constant. The dielectric constant of the prism is given by ε_0, θ is the incidence angle, and i is the imaginary unit. The dielectric constants of Ag, Ge, and Ni used in the computation are $\varepsilon_{Ag} = -16.0 + 0.6\mathrm{i}$, $\varepsilon_{Ge} = 29.89 + 8.37\mathrm{i}$, and $\varepsilon_{Ni} = -10.11 + 14.74\mathrm{i}$ for $\lambda = 633$ nm.[20] The reflectivity at the prism interfaces has been taken into account to calculate the reflection spectrum.

The influence of surface roughness can be taken into account *via* a variation of metal permittivity.[21] This will give rise to a small deviation Δk_{SP} from the SPP wave vector on smooth metal surfaces. The effective permittivity of metals with surface roughness is derived from $k_{SP}(\varepsilon_{eff}) = k_{SP}(\varepsilon_m) + \Delta k_{SP}$, where Δk_{SP} can be calculated using a formula derived previously.[22] By substituting the permittivity ε_m of the metal with ε_{eff} into eq 5, we can obtain the SPR spectrum by taking surface roughness into account.

Figure 3 plots angular dependent reflectivities of both experimental and theoretical results for all samples. Theoretical results for Samples 1−3 taking roughness into account are denoted as "Theory w/t roughness" while those without roughness as "Theory w/o roughness". As shown in Figure 3a, the resonant angle of the calculated curve without roughness for Sample 1 has been shifted from ~42.0° to ~42.05° both in calculations with roughness taken into account and in the experimentally obtained values. The roughness of Sample 2, as shown in Figure 3b, also caused a small displacement of resonant angle from ~42.05° to ~42.07° in the theoretical curves, and ~42.1° in the experimental curve, respectively. Figure 3c shows that the rougher surface of Sample 3 has obviously resulted in a relatively larger displacement of the resonant angle from ~42.0° to ~42.41° if roughness is included in the calculations, with a value of ~42.15° in the experimental curve. It is interesting to note that Samples 1 and 2 exhibit almost the same angular shifts of ~0.05°, although the rms roughness of Samples 1 and 2 are significantly different. This implies that the surface roughness effect is not a dominant factor in determining the resonance angle for a small roughness value for a metal thickness in the region of critical coupling.

The angular FWHMs of the experimental and theoretical curves taking into account roughness for all samples are correspondingly larger than those of the curves without roughness as shown in Figure 3a−c. It indicates that surface roughness leads to an increase of the losses of surface plasmon by broadening the SPR curves in terms of FWHM, due to scattering at the interface. Further analytical calculations showed that the surface roughness has an about 10-fold larger effect on the displacement of the resonant angle than the film thickness for the cases analyzed in this study. The calculated and measured angular resonance shifts and the broadening of SPR curves are qualitatively in agreement with observations of the roughness effect in the literature.[23] The angular FWHMs of Sample 1 are smaller in all the experimental and calculated SPR curves than those of Sample 3. It shows that the Ni layer is effective in enhancing the surface plasmon resonance and thus its sensitivity. On the other hand, Sample 2 exhibits a larger FWHM in the measured and theoretical curve without roughness, but a smaller value in the theoretical curve with roughness, compared to the plain Ag film

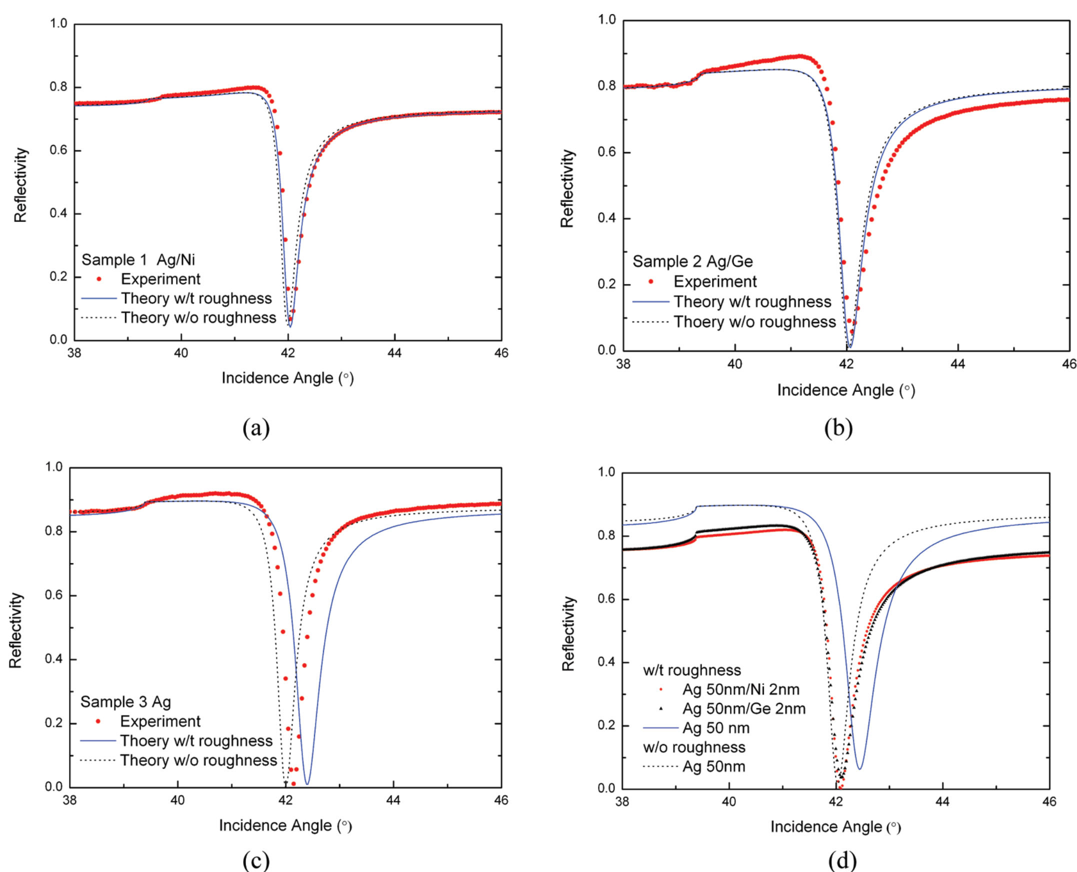

Figure 3. The SPR reflectivity curves of (a) Sample 1, (b) Sample 2, and (c) Sample 3. The dotted lines (●) represent the experimental curves; the solid lines represent the theoretical curves with roughness; and the dash-dotted lines represent the theoretical curves without roughness. (d) The theoretical SPR reflectivity curves for Ag 50 nm/Ni 2 nm, Ag 50 nm/Ge 2 nm, Ag 50 nm with roughness and Ag 50 nm without roughness.

of Sample 3. On the basis of a number of different film measurements, for practical applications we can conclude that a Ge seed layer degrades the SPR response.

Table 3 also compares the overall performance of SPR in terms of FOMs for these three samples. When a perfectly flat surface is employed, Sample 1 exhibits almost the same FOM (2.37) as Sample 3 (2.38), but a higher one than Sample 2 (1.86). Since there is no roughness taken into account, the smaller FOM in Ag/Ge film is obviously caused by the inherent dielectric properties of the Ge material, leading to increased absorptive damping. The smaller FOM observed in the experimental data in the Ag/Ge sample (1.35) than that in the pure Ag film (2.24) indicates that even though a Ge seed layer can reduce the Ag film roughness, it unfortunately deteriorates the overall surface plasmon response, due to the higher loss of Ge than Ag in the frequency range of interest. On the other hand, Sample 1 exhibits larger FOMs than Sample 3 in both the experimental data and the calculated result with roughness being taken into account. This clearly shows that Ni film has led to a better SPR sensitivity than pure Ag film in terms of FOM by reducing the surface roughness while adding no extra damping to the Ag film, which is the main conclusion of our work.

To exclude the effect of small layer thickness difference and further corroborate the discussions above, four samples with identical thickness for corresponding layers have been simulated. These four samples include Ag 50 nm/Ni 2 nm (w/t roughness), Ag 50 nm/Ge 2 nm (w/t roughness), Ag 50 nm (w/t roughness), and Ag 50 nm (w/o roughness). The roughness values of Ag

TABLE 3. Key Features of SPR Experimental and Theoretical Reflectivity Curves

	resonance angle (deg)			angular FWHM (deg)			figure of merit (FOM)		
sample no.	expt.	theory w/t roughness	theory w/o roughness	expt.	theory w/t roughness	theory w/o roughness	expt.	theory w/t roughness	theory w/o roughness
Sample 1, Ag/Ni	42.05	42.05	42.0	0.42	0.41	0.39	2.34	2.30	2.37
Sample 2, Ag/Ge	42.1	42.07	42.05	0.70	0.54	0.53	1.35	1.82	1.86
Sample 3, Ag	42.15	42.41	42.0	0.44	0.56	0.42	2.24	1.75	2.38

TABLE 4. Key Features of SPR Theoretical Curves for the Samples with Identical Thickness

sample no.	resonance angle (deg)	angular FWHM (deg)	figure of merit (FOM)
Ag 50 nm/Ni 2 nm	42.10	0.56	1.78
Ag 50 nm/Ge 2 nm	42.10	0.67	1.43
Ag 50 nm w/t roughness	42.43	0.71	1.32
Ag 50 nm w/o roughness	42.05	0.52	1.88

50 nm/Ni 2 nm, Ag 50 nm/Ge 2 nm and Ag 50 nm have been assumed to be the same as the AFM measurement results of Samples 1, 2 and 3, respectively. Figure 3d plots the calculated SPR reflectivity curves for these four samples while their key features are listed in Table 4. It shows that the presence of Ni enhances the SPR sensitivity, which is better than Ge and pure Ag film without any seed layer. For FOM values, the sample of Ni seed layer exhibits ~35% improvement compared to a Ag film with roughness being taken into account. The results based on these four samples give the same conclusions as those obtained based on Samples 1, 2, and 3.

The shape of the SPR reflectivity curve can be related to the propagation length of SPPs. Using a Lorentzian model,[24] the propagation length can be derived as

$$L_{SP} = \frac{[n_p^2 - \sin^2(\pi/4 - \theta_{res})]^{1/2}}{n_p k_0 \cos(\theta') \cos(\pi/4 - \theta_{res})\Delta\theta} \quad (6)$$

where $\theta' = \pi/4 - \sin^{-1}(\sin(\pi/4 - \theta_{res})/n_p)$, $\Delta\theta$ is the FWHM, and θ_{res} is the resonance angle. By using the experimental data, the propagation length of SPP approaches 18.8 μm for the Ag/Ni sample. From eq 6, the propagation length of SPPs is inversely proportional to the SPR peak width. However, it is important to note that while a seed layer can reduce the roughness of the metal surface, it can also lead to a decrease in the SPR coupling efficiency. This is shown in Figure 4a, which theoretically plots the reflectivity as a function of incidence angle at different seed layer thickness for Ag/Ni structures. To explain on the influence of the seed layer, a simple model was proposed to investigate the propagation length of SPPs on the metal with seed layers. Considering the SPPs propagating in the Ag/Ni and Ag/Ge structures, their magnetic field amplitudes can be derived as $\mathbf{H}_{SP} = H_0 \exp(jk_{SP,r}x)$, where H_0 denotes the amplitude at $x = 0$, and $k_{SP,r}$ represents the complex wave vector of SPPs. The propagation length of SPPs is given as $L_{SP} = {}^1/_2\mathrm{Im}(k_{SP,r})$. Figure 4b plots the SPP propagation length as a function of the thickness of Ni and Ge, while the thickness of Ag is fixed as a constant of 50 nm. The surface roughness of Ag/Ni and Ag/Ge is neglected due to their ultrasmooth surfaces. For comparison, Ag of 50 nm thickness w/t and w/o roughness are represented by dark solid and dashed lines, respectively. The roughness of the Ag surface in the computation is extracted from the experimental data. The inset in Figure 4b represents the field distribution of SPPs (the eigenmode of the structure) for Ag/Ni waveguides. We note that for the particular roughness values taken from the experimental data, although the addition of Ge and Ni may bring about absorption loss, SPPs can propagate longer distances for Ag/Ge and Ag/Ni than that for Ag with roughness. The model predicts a SPP propagation length of 16.6 μm for Ag/Ni with a seed layer thickness of 2 nm, comparable to the experimental value. Note the model only applies for predicting the propagation length while the seed layer is thin enough so that the incident light can efficiently couple to SPPs.

CONCLUSIONS

We have demonstrated smooth silver film deposition using Ni and Ge as seed layers on both Si(100) and quartz substrates. Values of ~0.7 nm and ~1.3 nm in terms of surface roughness (rms) have been achieved for Ag films with Ge and Ni seed layers, respec-

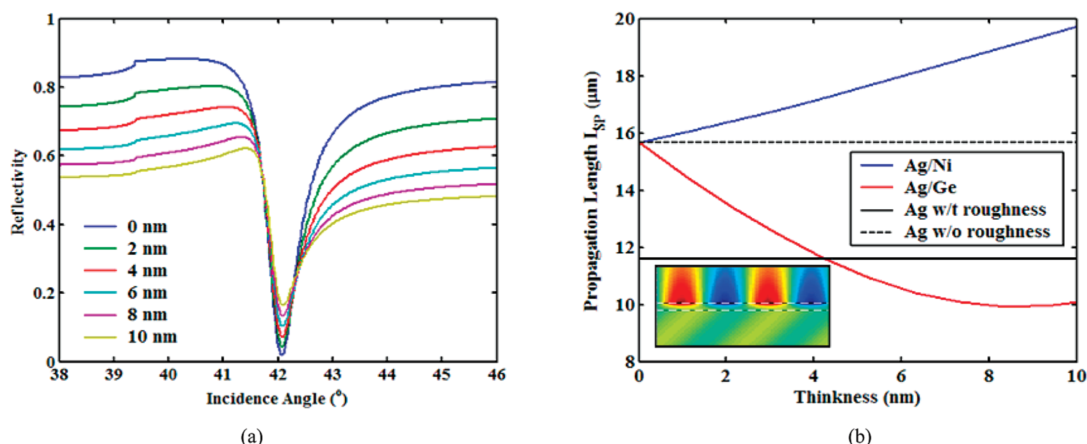

Figure 4. (a) SPR reflectivity spectra of Ag/Ni varying with the thickness of Ni. (b) Propagation length as a function of the seed layer thickness. The blue, red, and dark solid lines denote Ag/Ni, Ag/Ge, and Ag with roughness, respectively, while the dark dashed line represents Ag without surface roughness. The inset shows the magnetic field distribution in the multilayer waveguide.

tively. Both experimental and theoretical studies of key features, such as resonance angle, FWHM, and FOM of surface plasmon resonance have shown that Ni as a seed layer enhances the SPR sensitivity of the Ag film. In comparison, the experimental results show the Ge seed layer has deteriorated SPR, even though it improves the surface roughness of the Ag films. The results demonstrate that Ni is a promising seed layer for the generation of ultrasmooth Ag films for plasmonic and metamaterials applications.

METHODS

Both Si and quartz substrates were used in the experiment. The Si substrates with a size of 25 mm × 25 mm were diced from Si(100) wafers of 0.5-mm thickness with native oxide layers (~1 nm thick). The quartz substrates have a dimension of 15 mm (L) × 15 mm (W) × 0.4 mm (H) and a refractive index of 1.46. Prior to the thin film deposition, the substrates were cleaned by a standard Piranha solution. Both Ag/Ni and Ag/Ge films were deposited sequentially on both silicon and quartz substrates without breaking vacuum in an Edwards Auto306 electron-beam evaporator at a base pressure of about 5×10^{-7} mbar. The evaporation rate was controlled at 0.1 nm/s for Ni and Ge and 0.2 nm/s for Ag. Variable angle spectroscopic ellipsometry (WVASE32, J. A. Woollam) was used to characterize film thickness. Data were acquired by scanning over the angle range from 65° to 75° in steps of 5° over the spectral range from 300 to 800 nm in steps of 2 nm. High-resolution X-ray specular reflectivity of Ag/Ge and Ag films were measured by high resolution X-ray reflectometry (HR-XRR) at a grazing incidence angle in the X-ray beamline from a synchrotron light source (700 MeV, 300 mA).[25] The diffractometer was a Huber 4-circle system 90000−0216/0 with a high-resolution step size of 0.0001° for ω and 2θ circles. The thickness of each layer (Ag, Ni and Ge) was obtained by the best-fittings of simulation and experiment data. The surface topography of the deposited Ag/Ni, Ag/Ge, and bare Ag films was characterized by a multimode atomic force microscope (AFM) from Digital Instruments in tapping mode. The samples were scanned over a size of 1 μm^2 at a tip velocity of 2 μm/s and a corresponding scan rate of 1 Hz. Surface plasmon resonance (SPR) spectroscopy has been conducted by a customized Kretschmann SPR instrument, which has been detailed in the literature.[26] Briefly, the beam of a linearly polarized He−Ne laser light (5 mW, $\lambda = 632.8$ nm) is modulated by a chopper and passes through two polarizers to make the intensity and the plane of polarization of the laser adjustable. The sample, BK 7 prism, and photodiode detector are mounted onto the two coaxial arms of a goniometer for precise angle scan of incidence and reflection beam. Surface plasmon is excited by coupling laser light through the BK 7 prism. The reflected laser light is measured by the detector through a lock-in amplifier. All the depositions and characterizations were performed at room temperature.

Acknowledgment. This work was financially supported by Agency for Science, Technology and Research (A*STAR), and by the UK Physical Sciences and Engineering Research Council (EPSRC). We thank S. L. Teo and A. B. Chew for their support in the sample processing.

REFERENCES AND NOTES

1. Fang, N.; Lee, H. S.; Sun, C.; Zhang, X. Sub-diffraction-limited Optical Imaging with a Silver Superlens. *Science* **2005**, *308*, 534–537.
2. Valentine, J.; Zhang, S.; Zentgraf, T.; Ulin-Avila, E.; Genov, D. A.; Bartal, G.; Zhang, X. Three-Dimentional Optical Metamaterial with a Negative Refractive Index. *Nature* **2008**, *455*, 376–379.
3. Chaturvedi, P.; Wu, W.; Logeeswaran, V. J.; Yu, Z. N.; Islam, M. S.; Wang, S. Y.; Williams, R. S.; Fang, N. X. A Smooth Optical Superlens. *Appl. Phys. Lett.* **2010**, *96*, 043102.
4. Zhang, X.; Liu, Z. W. Superlenses to Overcome the Diffraction Limit. *Nature* **2008**, *7*, 435–441.
5. Sonnefraud, Y.; Verellen, N.; Sobhani, H.; Vandenbosch, G. A. E.; Moshchalkiv, V. V.; Van Dorpe, P.; Nordlander, P.; Maier, S. A. Experimental Realization of Subradiant, Superradiant, and Fano Resonances in Ring/Disk Plasmonic Nanocavities. *ACS Nano* **2010**, *4*, 1664–1670.
6. Dolling, G.; Enkrich, C.; Wegener, M. Low-loss Negative-Index Metamaterial at Telecommunication Wavelength. *Opt. Lett.* **2006**, *31*, 1800–1801.
7. Chettiar, U. K.; Kildishev, A. V.; Yuan, H. K.; Cai, W. S.; Xiao, S. M.; Drachev, V. P.; Shalaev, V. M. Dual-band Negative Index Metamaterial: Double Negative at 813 nm and Single Negative at 772 nm. *Opt. Lett.* **2007**, *32*, 1671–1673.
8. Tsuda, Y.; Omoto, H.; Tanaka, K.; Ohsaki, H. The Underlayer Effects on The Electrical Resistivity of Ag Thin Film. *Thin Solid Films* **2006**, *502*, 223–227.
9. Johnson, P. B.; Christy, R. W. Optical Constants of the Noble Metals. *Phys. Rev. B* **1972**, *6*, 4370–4379.
10. Edwards, H. W.; Petersen, R. P. Reflectivity of Evaporated Silver Films. *Phys. Rev.* **1936**, *50*, 871.
11. Yuan, H. K.; Chettiar, U. K.; Cai, W. S.; Kildishev, A. V.; Boltasseva, A.; Drachev, V. P.; Shalaev, V. M. A Negative Permeability Material at Red Light. *Opt. Express* **2007**, *15*, 1076–1083.
12. Chi, Y.; Lay, E.; Chou, T. Y.; Song, Y. H.; Carty, A. Deposition of Silver Thin Films Using the Pyrazolate Complex $[Ag(3,5\text{-}(CF_3)_2C_3HN_2)]_3$. *Chem. Vap. Deposition* **2005**, *11*, 206–212.
13. Jing, F.; Tong, H.; Kong, L.; Wang, C. Electroless Gold Deposition on Silicon (100) Wafer Based on A Seed Layer of Silver. *Appl. Phys. A: Mater. Sci. Process.* **2005**, *80*, 597–600.
14. Yin, L. L.; Vlasko, V. K. V.; Pearson, J.; Hiller, J. M.; Hua, J.; Welp, U.; Brown, D. E.; Kimball, C. W. Subwavelength Focusing and Guiding of Surface Plasmons. *Nano Lett.* **2005**, *5*, 1399–1402.
15. Kapaklis, V.; Poulopoulos, P.; Karoutsos, V.; Manouras, Th.; Politis, C. Growth of Thin Ag Films Produced by Radio Frequency Magnetron Sputtering. *Thin Solid Films* **2006**, *510*, 138–142.
16. KunDu, S.; Hazra, S.; Banerjee, S.; Sanyal, M. K.; Mandal, S. K.; Chaudhuri, S.; Pal, A. K. Morphology of Thin Silver Film Grown by DC Sputtering on Si(001). *J. Phys. D: Appl. Phys.* **1998**, *31*, L73–L77.
17. Logeeswaran, V. J.; Chan, M. L; Bayam, Y.; Islam, M. S.; Horsley, D. A.; Li, X.; Wu, W.; Wang, S. Y.; Williams, R. S. Ultrasmooth Metal Surfaces Generated by Pressure-Induced Surface Deformation of Thin Metal Films. *Appl. Phys. A: Mater. Sci. Process.* **2007**, *87*, 187–192.
18. Nagpal, P.; Lindquist, N. C.; Oh, S. H.; Norris, D. J. Ultrasmooth Patterned Metals for Plasmonics and Metamaterials. *Science* **2009**, *325*, 594–597.
19. Logeeswaran, V. J.; Nobuhiko, P. K.; Islam, M. S.; Wu, W.; Chaturvedi, P.; Fang, N. X.; Wang, S. Y.; Williams, R. S. Ultrasmooth Silver Thin Fimls Deposited with a Germanium Nucleation Layer. *Nano Lett.* **2009**, *9*, 178–182.
20. Palik, E. D., Ed. *Handbook of Optical Constants of Solids*; Academic Press: New York, 1991.
21. Kolomenski, A.; Kolomenskii, A.; Noel, J.; Peng, S. Y.; Schuessler, H. Propagation Length of Surface Plasmons in a Metal Film with Roughness. *Appl. Opt.* **2009**, *48*, 5683–5691.
22. Fontana, E.; Pantell, R. H. Characterization of Multilayer Rough Surfaces by Use of Surface-Plasmon Spectroscopy. *Phys. Rev. B* **1988**, *37*, 3164–3182.

23. Hoffmann, A.; Lenkefi, Z.; Szentirmay, Z. Effect of Roughness on Surface Plasmon Scattering in Gold Films. *J. Phys.: Condens. Matter* **1998**, *10*, 5503–5513.
24. Kyung, M. B.; Soon, J. Y.; Kim, D. Y. Effect of Surface Roughness on the Extinction-Based Localized Surface Plasmon Resonance Biosensors. *Appl. Opt.* **2008**, *47*, 5886–5892.
25. Yang, P.; Moser, H. O. High Resolution Reflectometry at Singapore Synchrotron Light Source. *Advances in Synchrotron Radiation*; World Scientific Publishing Company: Singapore, 2008; Vol. 1, pp 105−113.
26. Knoll, W. Interfaces and Thin Films as Seen by Bound Electromagnetic Waves. *Annu. Rev. Phys. Chem.* **1998**, *49*, 569–638.